

Maser emission of the most abundant SiO isotopomers in O-rich stars

J. R. Rizzo¹, C. García Miró² and J. Cernicharo³

¹ Centro de Astrobiología (INTA-CSIC), E-28850 Torrejón de Ardoz, Spain

² Madrid Deep Space Communications Complex (NASA-INTA), E-28294 Robledo de Chavela, Spain

³ Instituto de Ciencias de Materiales de Madrid (CSIC), E-28049, Madrid, Spain

Abstract

SiO maser emission constitutes one of the most puzzling cases in spectroscopy. The overall inversion of the rotational transitions in each vibrational ladder is rather well understood. However, there are a number of anomalies in specific rotational transitions that are still unexplained. O-rich stars are probably the most powerful maser emitters known to date, and therefore the best candidates to model the SiO maser emission at different rotational and vibrational levels. In order to properly tackle the SiO excitation problem, it is vital to simultaneously observe a large number of SiO (and isotopomers) lines in a large and varied sample of sources. We profit the availability of new wideband backends to carry out a deep survey of ²⁸SiO, ²⁹SiO, and ³⁰SiO maser emission, in a sample of 67 evolved O-rich stars. The survey was done using the DSS-54 antenna at the Madrid Deep Space Communications complex in Robledo, and the IRAM 30m radio telescope at Pico Veleta. A total of 61 lines were observed, including rotational transitions from $J = 1 \rightarrow 0$ to $J = 5 \rightarrow 4$, for vibrational levels from 0 to 6. In this contribution, overall results of the survey are presented.

1 Introduction

Maser emission in ²⁸SiO rotational transitions of vibrationally excited states is very ubiquitous and intense in O-rich stars. A number of maser lines have been detected in the ground and excited vibrational states of the rare isotopomers ²⁹SiO and ³⁰SiO [1, 4]. Besides the overall inversion of the rotational levels in each vibrational ladder, the SiO emission displays puzzling anomalies in some specific rotational lines, such as drastic changes in intensity from one rotational line to the next within the same v -state. This is difficult to be explained by standard radiative and collisional pumping models. In some cases, they have been interpreted as a result of overlaps between the ro-vibrational lines of the ²⁸SiO, ²⁹SiO and ³⁰SiO [1, 2].

Some of the best surveys include the observation of 11 lines of ^{28}SiO in 6 evolved stars [10], the line survey in the red supergiant VY CMa [2], the study of 12 sources [7], the survey of six $J = 1 \rightarrow 0$ transitions in various vibrational states of ^{28}SiO and ^{29}SiO [3], and a study of the $J = 1 \rightarrow 0$ $v = 1$ and 2 lines [5]. Most of the other studies, however, have been carried out in different epochs, with different instruments and, sometimes, without a complete coverage of the rotational transitions from the different vibrational levels of SiO. Due to the variability of the SiO maser emission and to the complexity of the physics of stellar pulsation (which is in turn associated to the line pumping), the observations gathered in different epochs cannot be compared to infer robust conclusions about the excitation of SiO.

To discriminate between the different physical processes leading to the population inversion of the SiO energy levels, and to retrieve key information about the physical conditions of the gas in the region between the photosphere and the dust growth zone, it is necessary to have the most complete, simultaneous and homogeneous sample of the SiO rotational emission in the different vibrational states. The current availability of wideband backends spanning several GHz of instantaneous bandwidths make possible nowadays this kind of studies. These backends permit the simultaneous observation of multiple spectral lines, saving observing time and minimizing the impact of the uncertainties in the calibration and pointing on the determination of physical parameters and modeling.

We report here the preliminary results of a maser line survey towards a sample of evolved O-rich stars, in the SiO, ^{29}SiO , and ^{30}SiO isotopomers. The selected sources (67 in total) span different mass losses, temperatures, and C/O abundance ratios. This work also provides valuable information about the molecular content of these objects. The survey was done using one of the 34 m antenna of the Madrid Deep Space Communications Complex (hereafter MDSCC) and the IRAM 30 m radio telescope at Pico Veleta. It includes 66 transitions from $J = 1 \rightarrow 0$ to $5 \rightarrow 4$, and $v = 0$ to 6. A full description of the results are planned to be submitted to a subsequent paper.

2 Observations

One of the 34 m antenna of the MDSCC was employed in the first part of the survey to observe the $J = 1 \rightarrow 0$ lines, at a wavelength of 7 mm (~ 43 GHz). Based on these initial results, we observed the most relevant sources in the $J = 2 \rightarrow 1$ to $5 \rightarrow 4$, at wavelengths of 3, 2 and 1 mm, using the 30 m IRAM radio telescope. The MDSCC observations were done between March and July 2012, and the IRAM observations in August 2012. A total of 67 stars have been observed. The Table 1 summarizes their coordinates, the telescope/s used, as well as the detection, if any, of maser lines.

For the MDSCC antenna, the new wideband backend was employed [9], attached to the Q-band receiver [8]; the resulting system temperature varied between 90 and 130 K. For the IRAM antenna, the FTS backend was used, attached to the EMIR receiver [6]. Integration times were between 5 and 36 minutes, reaching *rms* noise as low as 6 mJy. The Q-band receiver is able to record both circular polarizations, while EMIR records lineal polarizations.

Table 1: Sources observed

Source	RA (J2000) hh:mm:ss.ss	Dec (J2000) ±dd:mm:ss.ss	V_{LSR} km s ⁻¹	Telescope	detect.	Source	RA (J2000) hh:mm:ss.ss	Dec (J2000) ±dd:mm:ss.ss	V_{LSR} km s ⁻¹	Telescope	detect.
Y Cas	00:03:21.40	+55:40:52.2	-17.0	MDSCC	Y	R Leo	09:47:33.49	+11:25:43.7	-1.0	both	Y
IRC+40004	00:06:53.24	+43:05:03.0	-19.7	MDSCC	N	U Hya	10:37:33.27	-13:23:04.4	-30.3	MDSCC	N
T Cas	00:23:14.27	+55:47:33.2	1.0	both	Y	R UMa	10:44:38.91	+68:46:32.9	40.0	MDSCC	N
R And	00:24:01.97	+38:34:40.3	-16.0	MDSCC	N	W Leo	10:53:37.42	+13:42:55.2	51.0	MDSCC	Y
IRC+10011	01:06:25.98	+12:35:53.0	9.0	both	Y	R Com	12:04:15.43	+18:46:55.8	-7.0	MDSCC	N
IRC+30021	01:11:15.94	+30:38:06.0	-39.3	MDSCC	Y	R Vir	12:38:30.37	+06:59:17.9	-28.2	MDSCC	Y
H2O125.6	01:16:37.16	+64:50:39.1	-53.0	MDSCC	N	T Com	12:58:38.92	+23:08:21.5	28.0	both	Y
S Cas	01:19:41.99	+72:36:40.8	-30.0	both	Y	RT Vir	13:02:37.78	+05:11:07.5	13.0	MDSCC	Y
IRC+50049	01:58:41.77	+45:26:16.2	4.4	MDSCC	Y	R Hya	13:29:42.87	-23:16:51.7	-5.0	MDSCC	Y
W And	02:17:33.24	+44:18:23.0	-34.0	MDSCC	Y	W Hya	13:49:02.07	-28:22:02.7	38.8	MDSCC	Y
O Cet	02:19:20.78	-2:58:39.5	45.0	both	Y	RX Boo	14:24:11.63	+25:42:13.4	-2.0	both	Y
S Per	02:22:51.71	+58:35:11.5	-38.0	both	Y	RS Vir	14:27:15.40	+04:40:28.3	1.0	MDSCC	Y
IRC+60092	02:35:46.01	+65:09:41.1	23.1	MDSCC	Y	S Crb	15:21:23.96	+31:22:02.6	1.0	both	Y
02395+624	02:43:28.10	+62:57:05.6	-70.0	MDSCC	N	WX Ser	15:27:47.04	+19:33:51.7	7.0	both	Y
02404+215	02:43:16.20	+22:03:34.6	-39.0	MDSCC	N	U Ser	16:07:17.67	+09:55:52.5	-16.0	both	Y
RU Ari	02:44:45.18	+12:19:08.2	20.0	MDSCC	Y	U Her	16:25:47.47	+18:53:32.9	-16.0	both	Y
T Ari	02:48:19.74	+17:30:33.8	-5.0	IRAM	Y	R Umi	16:29:57.90	+72:16:49.2	-12.0	both	Y
02547+1106	02:57:27.48	+11:18:05.7	-5.0	IRAM	Y	IRC+20326	17:31:54.48	+17:45:28.7	-4.0	MDSCC	N
IRC+20052	03:01:34.64	+21:48:12.3	-36.5	MDSCC	Y	VX Sgr	18:08:04.05	-22:13:26.6	7.5	both	Y
AFGL490	03:27:37.61	+58:46:58.0	33.0	MDSCC	N	AFGL2139	18:23:17.37	-13:42:48.4	37.0	MDSCC	Y
NML Tau	03:53:28.87	+11:24:21.7	33.0	IRAM	Y	V1111 Oph	18:37:19.26	+10:25:42.2	-31.4	both	Y
IRC+30072	04:09:36.97	+33:29:37.4	7.0	IRAM	Y	R Aql	19:06:22.25	+08:13:48.0	48.3	both	Y
TW Cam	04:20:47.63	+57:26:28.5	-50.0	IRAM	N	W Aql	19:15:23.31	-07:02:49.8	-16.0	MDSCC	N
S Tau	04:29:11.74	+09:56:43.4	17.0	IRAM	Y	χ Cyg	19:50:33.92	+32:54:50.6	8.3	both	Y
IRC+10066	04:38:14.56	+08:20:09.2	-44.0	IRAM	Y	TW Aql	19:51:00.83	+13:59:14.2	38.0	MDSCC	N
TX Cam	05:00:50.39	+56:10:52.6	9.0	IRAM	Y	RR Aql	19:57:36.06	-01:53:11.3	31.0	both	Y
IRC+60154	05:19:52.56	+63:15:55.8	40.7	IRAM	Y	IRC-10529	20:10:27.61	-06:16:12.7	-15.1	MDSCC	Y
HK Ori	05:31:28.05	+12:09:10.3	11.0	IRAM	Y	NML Cyg	20:46:25.54	+40:06:59.4	-1.2	both	Y
α Ori	05:55:10.31	+07:24:25.0	3.0	both	Y	T Cep	21:09:31.78	+68:29:27.2	0.0	both	Y
U Ori	05:55:49.17	+20:10:30.7	-40.2	both	Y	μ Cep	21:43:30.46	+58:46:48.2	24.0	both	Y
VY CMa	07:22:58.33	-25:46:03.2	22.0	both	Y	AFGL2999	22:57:40.99	+58:49:12.5	-58.0	both	Y
S CMi	07:32:42.79	+08:19:07.0	58.0	MDSCC	Y	R Aqr	23:43:49.46	-15:17:04.1	-28.0	both	Y
RS Cnc	09:10:38.83	+30:57:48.6	7.0	MDSCC	Y	R Cas	23:58:24.87	+51:23:19.7	24.0	both	Y
R Lmi	09:45:34.21	+34:30:43.9	3.0	MDSCC	Y						

3 Results

The resulting spectra can be reduced to a number of 458, containing 9 to 14 maser lines each. Over a resulting total of 4716 lines, we have 1525 positive detections. These detections are predominantly from $v = 1$ in the ^{28}SiO species. We remark the first detection of a highly vibrationally line ($v = 6$) in the sample. The Fig. 1 depicts the full range spectrum of one of the sources (IRC+10011 = WX Psc) in the $J = 1 \rightarrow 0$ transitions. In this case, six lines are detected over a total of ten possible lines.

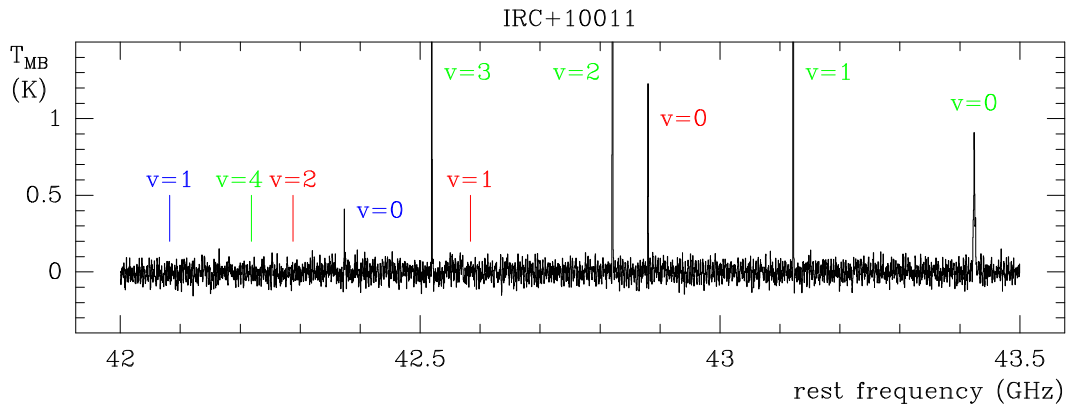


Figure 1: A full range spectrum of IRC+10011 in the $J = 1 \rightarrow 0$ lines.

The Fig. 2 shows representative examples of the line shapes. Source name is indicated on the upper left and the transition in the upper right corner of each panel. In the case of S Per the spectrum is dominated by two peaks. In the case of S Cas, the shape of a truncated parabolic and wide line is indicative of thermal emission from the circumstellar envelope as a whole. In O Cet the $^{28}\text{SiO } J = 4 \rightarrow 3, v = 2$ line displays a component at $\sim 57 \text{ km s}^{-1}$ which is well outside the velocity range of the thermal line; the $J = 4 \rightarrow 3, v = 1$ line (lower left panel) has a Gaussian shape, and is centered at the star velocity. The line depicted for IRC+10011 is a paradigmatic very narrow maser line. And finally, the line displayed for NML Tau is the result of the superposition of both the thermal component and at least one maser component.

Usually, the SiO (and isotopomers) maser lines in evolved stars are variable. One of the most clear examples is shown in Fig. 3, where the $^{30}\text{SiO } J = 1 \rightarrow 0, v = 0$ line dramatically changed in just two weeks. A significant part of the maser lines are often linearly and circularly polarized. The IRAM spectra contains valuable information about lineal polarization of these sources, although it is not possible to derive the Stokes parameters. Even though, the simultaneous observations of both lineal polarizations during four consecutive nights allowed the discovery of highly polarized components. An example is shown in Fig. 4, where at least one of the components seen in the horizontal polarization (at $\sim 10 \text{ km s}^{-1}$) is virtually absent in the vertical polarization.

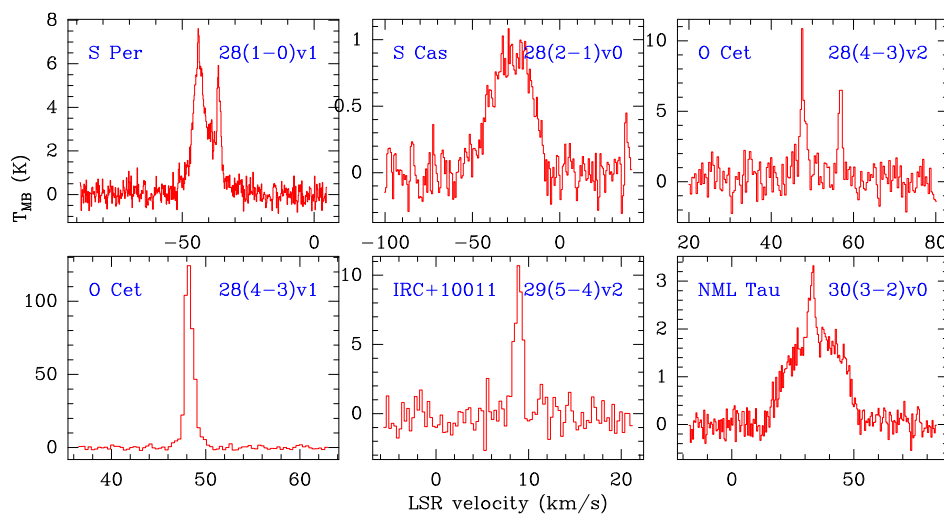


Figure 2: A sample of six different line profiles.

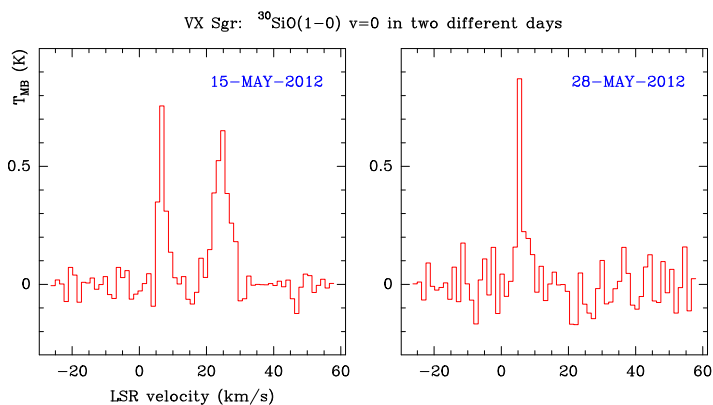


Figure 3: An example of variability. The $^{30}\text{SiO } J = 1 \rightarrow 0, v = 0$ line has been observed with a separation of only two weeks in VX Sgr, obtaining very different spectra.

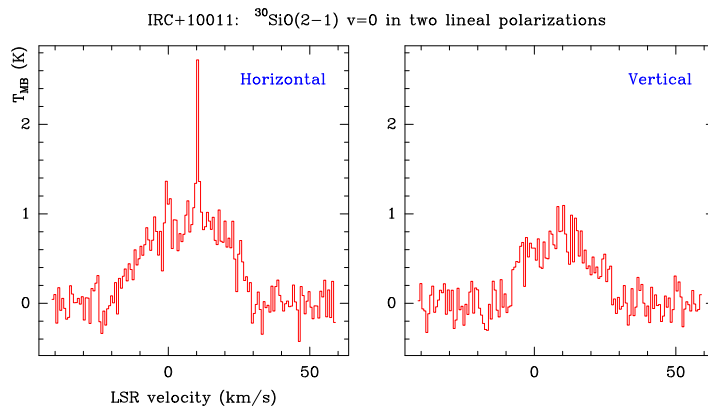


Figure 4: An example of a highly linearly polarized component, the $^{30}\text{SiO } J = 2 \rightarrow 1, v = 0$ line towards IRC+10011.

4 Concluding remarks

This sensitive survey allowed the detection of new SiO maser lines, some of them already predicted theoretically. This is the most complete of almost simultaneous maser lines in a rich sample of O-rich stars. The resulting database will be later used for a complete modeling of the SiO maser phenomenon in the extended atmospheres of evolved solar-like stars.

Although we do not derive Stokes parameters, some hints of both lineal and circular polarizations are also found. Finally, the survey also contains spectroscopic information about the content of molecular species related to the dust formation zone.

Acknowledgments

We acknowledge the kind and professional support of MDSCC and IRAM staffs during the observations. This work is supported by MICINN (Spain) grants CSD2009-00038, AYA2009-07304, and AYA2012-32032.

References

- [1] Cernicharo, J., & Bujarrabal, V. 1992, *ApJL*, 401, L109
- [2] Cernicharo, J., Bujarrabal, V., Santarén, J. L. 1993, *ApJL*, 407, L33
- [3] Cho, S.-H., Kaifu, N., Ukita, N. 1996, *A&AS*, 115, 117
- [4] González-Alfonso, E., Alcolea, J., Cernicharo, J. 1996, *A&A*, 313, L13
- [5] Kim, J., Cho, S.-H., Oh, C. S., Byun, D.-Y. 2010, *ApJS*, 188, 209
- [6] Klein, B., Krämer, I., Hochgürtel, S., et al. 2009, *Twentieth International Symposium on Space Terahertz Technology*, 199
- [7] Pardo, J. R., Cernicharo, J., González-Alfonso, E., Bujarrabal, V. 1998, *A&A*, 329, 219
- [8] Rizzo, J. R., & García-Miró, G. 2013, *Highlights of Spanish Astrophysics VII*, 904
- [9] Rizzo, J. R., Pedreira, A., Gutiérrez Bustos, M., et al. 2012, *A&A*, 542, A63
- [10] Schwartz, P. R., Zuckerman, B., & Bologna, J. M. 1982, *ApJL*, 256, L55